Kivisaari, Pyry; Oksanen, Jani

Resonance effects in the radiation transfer of thin-film intracavity devices

Published in:
Applied Physics Letters

DOI:
10.1063/5.0109763

Published: 07/11/2022

Document Version
Peer-reviewed accepted author manuscript, also known as Final accepted manuscript or Post-print

Please cite the original version:
Kivisaari, P., & Oksanen, J. (2022). Resonance effects in the radiation transfer of thin-film intracavity devices. *Applied Physics Letters*, *121*(19), Article 191101. https://doi.org/10.1063/5.0109763

Resonance effects in the radiation transfer of thin-film intracavity devices

Pyry Kivisaari* and Jani Oksanen
Engineered Nanosystems Group, Aalto University, P.O. Box 13500, FI-00076 Aalto, Finland

A great deal of interest has been recently directed at exploring how the performance of photovoltaic and thermophotovoltaic systems can benefit from the use of ultra-thin layers and near-field effects. Related questions on how radiation transfer is modified if both the source and sink of the radiation are located within an optical cavity have, however, received far less attention. This question is nevertheless particularly relevant in the field of electroluminescence-driven thermophotonics, which could substantially benefit from the possibility to boost the energy transfer by making use of optical cavities. To gain insight into this possibility, we deploy fluctuational electrodynamics and study the fundamental resonance effects in structures where the emitter and absorber layers are separated by a vacuum nanogap and bordered by high-efficiency mirrors. We obtain the expected result that resonance effects can strongly enhance the interactions at specific wavelengths and propagation angles. Moreover, we find that even after integrating over wavelength and propagation angle, (1) the total power emitted can be tuned by adjusting the cavity thickness and the optical cavity mode structure, and (2) thinning the active layer enhances its emission in the cavity, causing a sublinear dependence between the active layer thickness and its overall emission. In plain numbers, adjusting the cavity thickness produces non-monotonous changes of over 50 % in the total emission of thin layers. These observations apply also to absorption, which can become remarkably efficient even for an extremely thin absorber layer thanks to cavity effects.

The presently ubiquitous light-emitting diodes (LEDs) can be seen as thermodynamic engines capable of sustaining near-reversible conversion between electrical, thermal and optical energy [1–5]. In concrete terms, the underlying phenomenon of electroluminescence (EL) can thus in principle be utilized both to cool down an LED structure [6] and even to turn it into a heat engine [7]. While the basic understanding of these effects is becoming more mature, they still lack a direct experimental demonstration at practical operating powers. One of the recent approaches to achieve this has been the use of a double-diode structure (DDS), where the emitter and absorber are placed within the same semiconductor heterostructure to promote efficient optical transfer [8]. As the associated experimental studies related to the different thermodynamic operating modes of the devices are gathering pace [9–19], it is of importance to also study the fundamental performance limits of such structures. One of the obvious questions is, does the optical power transfer of a DDS depend on cavity resonances and in what magnitude?

In the more established photovoltaics research field, recent studies have shown that light trapping can lead to efficient absorption even when the absorbing layers are thinned down to a few hundred nanometers [20–23]. Such thin films are also known to modify the spontaneous emission rate due to changes in the optical environment [24], and this has been partly touched upon in the photovoltaics context with regards to photon recycling. More broadly, however, overall conclusions for the total angle- and energy-integrated emission rates of ultra-thin films and optical cavities are still somewhat incomplete, especially in the context of EL, where emission is generally possible in all directions. In other words, even if emission is well-known to be enhanced in specific directions and wavelengths in optical cavities, the resulting effect in the total emission rates is not fully established. In the thermophotonics context considered here, it would be particularly important to understand how the emission and absorption behave when the emitter and absorber are separated by a vacuum nanogap (necessary for sustaining a temperature difference) and placed in an intracavity structure with high-efficiency mirrors on both sides, as in Fig. 1. In particular, we are interested in the existence of fundamental resonance effects in the overall energy transfer (here generally meaning variations in the

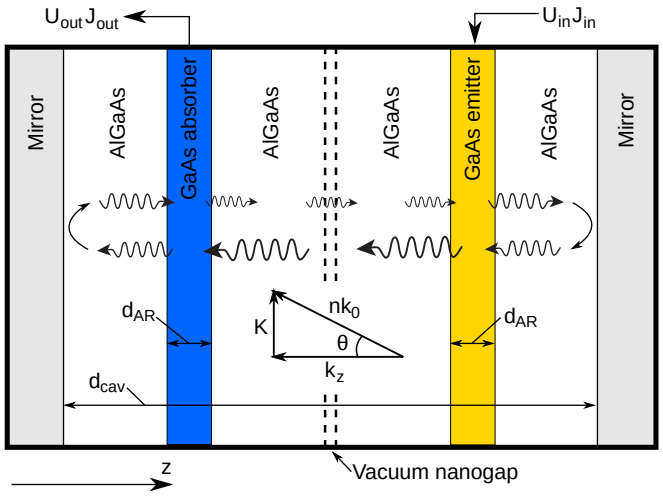

FIG. 1: The double-sided full cavity structure studied in this paper with mirrors on both sides. The GaAs layers are always centered in the cavities formed by the nanogap and each of the mirrors.

*Corresponding author. Email: pyry.kivisaari@aalto.fi

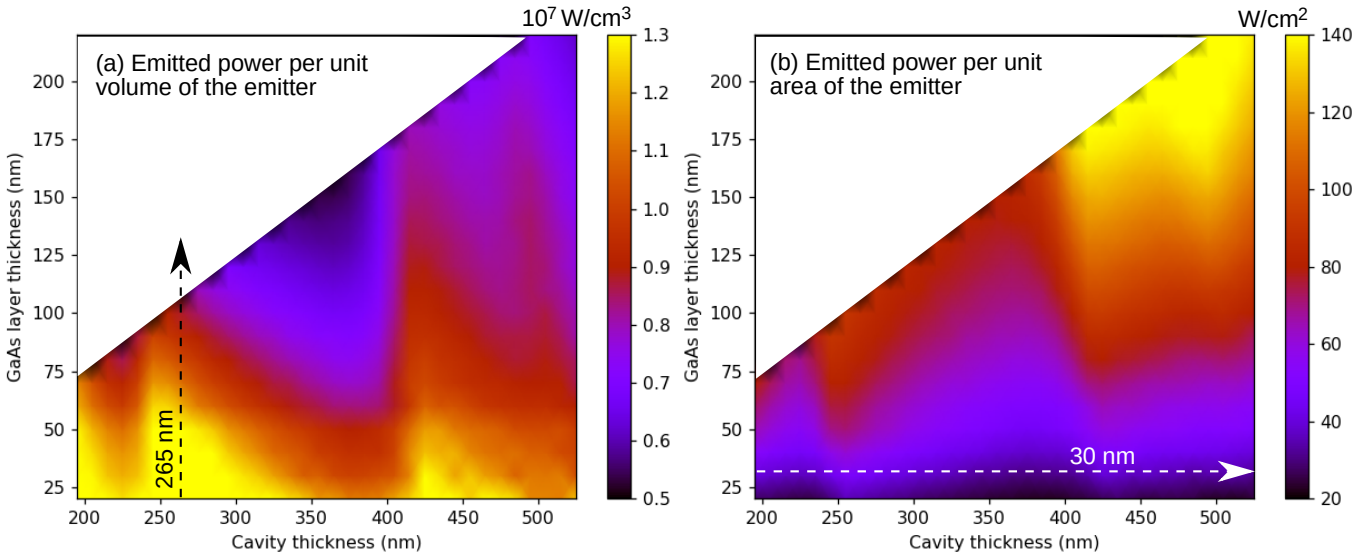

FIG. 2: (a) $R_{rad}(z)$ averaged over the emitting GaAs layer and (b) $R_{rad}(z)$ integrated over the emitting GaAs layer, both as a function of cavity thickness and GaAs layer thickness. In other words, (a) gives the optical power emitted by a unit volume and (b) the optical power emitted by a unit area. The white color in the upper left corner corresponds to the unfeasible case of the GaAs layers and vacuum gap together having a larger thickness than the complete cavity. The slight staircase pattern at the border is caused by the 10 nm step size between different thicknesses.

spontaneous emission rate and energy transfer caused by modifications in the optical cavity), when both the cavity and the emitter and absorber layers are shrunk towards and even well below the emission wavelength, and when all directions and wavelengths are accounted for.

Studying the energy transport in thermophotonic cavity structures in this level of detail requires treatments where both emission and absorption within the cavity are fully accounted for. Here, we use a variant of fluctuational electrodynamics (FED) developed in our previous works [25–27]. Using this framework, we calculate emission-absorption rates attained in double-sided cavities, studying both total rates (incorporating all wavelengths and propagation angles) and the underlying optical mode structures. The results are interpreted with the help of three guiding questions: (1) how large changes do cavity effects induce in the total angle- and energy-integrated rates, (2) how does the total emission rate of a thin layer depend on the cavity thickness, and (3) can one boost the emission and absorption rates by (somewhat counterintuitively) shrinking the active layers which, while decreasing their nominal emissivity, also enhances the optical power that can be present in the cavity?

To answer the questions presented above, we deploy the FED formulation reported e.g. in Refs. 25 and 26. The treatment is equivalent to more conventional FED formulations, but it is geared towards directly producing quantities familiar to device engineers. This is done through the use of photon numbers that separate between the local field strength and collective interference-corrected interactions as detailed below. Accordingly, FED is deployed to calculate the position-dependent net recombination-generation rates per unit volume (here in units of W/m^3) as

$$R_{rad}(z) = \int_0^\infty d\omega \int_0^\infty dK r(z, K, \omega) 2\pi K, \qquad (1)$$

where $\omega > 0$ is the angular frequency of light, K is the in-plane wave number (essentially fixing the propagation direction), and z is the position coordinate. The spectral recombination-generation rate r is calculated as $r = ds/dz$, where s is the spectral radiance propagating in the cavity, calculated from the local direction-specific photon numbers ϕ as [25]

$$s(z, K, \omega) = \frac{1}{2} \sum_{TE,TM} \hbar\omega v(z) \rho(z, K, \omega) [\phi(z, K, \omega) - \phi(z, K, -\omega)]. \qquad (2)$$

Here, $-\omega$ corresponds to modes propagating in the negative direction, $v = c/N$ (c speed of light in vacuum and N refractive index) is the speed of light in the medium, and ρ is the local density of states as defined in Ref. 26.

The photon numbers in Eq. (2) represent a complete solution to the inhomogeneous Maxwell's equations and thereby determine all emission and absorption processes taking place in the device. Here, they are calculated by following Ref. 25 and making use of the optical admittance method formulated in Ref. 27. More precisely, one calculates the full dyadic Green's function and the associated local, nonlocal and interference densities of states (ρ, ρ_{NL} and ρ_{IF}, respectively), which determine

the rightward and leftward photon numbers as

$$\phi(z,K,\pm\omega) = \frac{1}{\rho(z,K,\omega)} \times \int_{-\infty}^{\infty} \left[\rho_{NL}(z,K,\omega,z_0) \pm \rho_{IF}(z,K,\omega,z_0)\right] \eta(z_0,\omega) dz_0, \quad (3)$$

where η is the source term (describing the equilibrium photon number that the material would emit when filling all space) and z_0 are the source coordinates. Here, based on the arguments presented in Ref. 28, η is equal to the Bose-Einstein distribution with the photon chemical potential assumed equal to the local quasi-Fermi level separation ΔE_F for frequencies above the band gap and 0 otherwise, i.e.,

$$\eta(z,\omega) = \frac{1}{e^{(\hbar\omega - \Delta E_F)/(k_B T)} - 1}. \quad (4)$$

Simulations are carried out for the structure shown in Fig. 1 for a range of active region and cavity thicknesses d_{AR} and d_{cav}. The vacuum nanogap has a thickness of 50 nm and a permittivity equal to 1. To calculate the EL of the emitter, the temperature and quasi-Fermi level separation there are set to 400 K and 1.3 V, respectively. To focus on the fundamental resonance effects associated with EL and energy transfer (instead of quantitative predictions for device optimization), in the calculations we neglect the temperature dependence of the band gap and consider above-bandgap photon energies from 1.41 to 1.65 eV, and K values from 0 to $1.05 \times N_{GaAs} k_0$, where N_{GaAs} is the refractive index of GaAs and k_0 is the wave number in vacuum, thereby limiting the study to modes freely propagating in GaAs. Moreover, as this study focuses on how resonance effects affect the useful emission from emitter to absorber, the absorber is initially assumed not to emit light for simplicity. However, supplementary calculations performed for this study (not shown) indicate that, e.g., when the absorber is at 300 K and has a bias of 1.2 V (representing a plausible condition for thermophotonic energy harvesting), its above-bandgap EL is only less than 1 % of the above-bandgap EL from the emitter at 400 K and 1.3 V (note that thanks to the perfectly symmetric geometry, this difference is solely due to the different bias and temperature). Dielectric functions are taken from Refs. 29–31 with the exception that the dielectric function of Ag is multiplied by 100 to decrease mirror losses and thereby set the focus of the analysis to optical processes taking place inside the cavity, while still allowing a small amount of mirror loss to refrain from overtly ideal conditions. The implications of all these choices are discussed further below.

The optical power radiated by the emitter is illustrated in Fig. 2 as a function of cavity thickness (d_{cav}) and GaAs layer thickness (d_{AR}). More specifically, Fig. 2(a) shows the recombination rate $R_{rad}(z)$ averaged over the emitter layer, while Fig. 2(b) shows $R_{rad}(z)$ integrated over the emitter layer, thereby giving the total optical power emitted by the layer per unit area. In general,

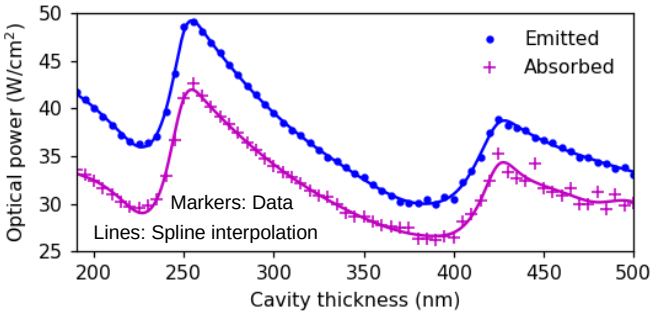

FIG. 3: Information in Fig. 2(b) plotted through the horizontal arrow there: optical power emitted by a 30 nm thick GaAs layer as a function of cavity thickness. The figure also shows the optical power absorbed by the GaAs absorber layer.

Fig. 2 answers question (1) of the introduction by clearly showing that resonance effects do not average out after performing the integrations over ω and K in Eq. (1). If resonance effects canceled out, Fig. 2(a) would exhibit roughly constant values and Fig. 2(b) would show a linear dependence on the GaAs layer thickness (until notable reabsorption would start taking place) with no dependence on the cavity thickness. Here, Fig. 2(a) indicates that the thinner the GaAs layer, generally the larger the R_{rad}, hence providing a quantitative illustration of the Purcell effect. Also, R_{rad} in Fig. 2(a) reaches several local maxima at certain cavity thicknesses. Figure 2(b) indicates that after integrating R_{rad} over the GaAs layer, thicker GaAs layers still generally emit higher total optical powers. However, an intricate dependence on both the GaAs layer and the cavity thickness remains also in Fig. 2(b) that can be studied in more detail through 1D graphs that give more quantitative insight.

First to explore the effects of cavity thickness, Fig. 3 repeats the information of Fig. 2(b) along the horizontal line marked in Fig. 2(b), i.e., by keeping the GaAs layer 30 nm thick and varying the cavity thickness. Also the optical power absorbed by the absorber layer is shown in the figure (with the difference explained by absorption by the mirrors). The small fluctuation in the absorption values at large cavity thicknesses is expected to result from the numerical integration in Eq. (1), where integrating with fixed ω and K grids over the shifting emission/absorption peaks produces such small fluctuations. Figure 3 answers question (2) of the introduction by demonstrating that the optical power transferred from emitter to absorber has a major non-monotonous dependency on the cavity thickness. The maximum values reached at around 265 nm are roughly 50 % higher than the minimum values at 370 nm, and there are two clear local maxima within the cavity thickness range considered in Fig. 3 (265 and 430 nm). For reference, we have calculated corresponding values for a GaAs layer thickness of 300 nm, i.e., the layer thickness in Fig. 3 multiplied by 10, and the highest values we obtain there are roughly 170 W/cm^2 (note that the cavity thickness

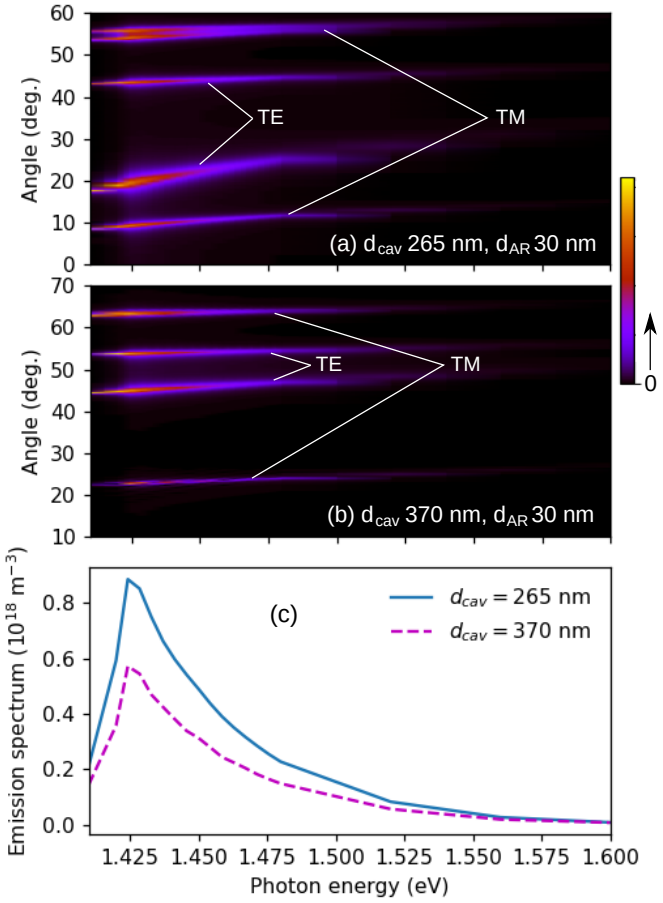

FIG. 4: (a-b) Spectral recombination rate $r(z, K, \omega)$ averaged over the emitter layer, with the cavity and GaAs layer thicknesses given in the figures, and (c) emission spectra calculated by integrating the quantities in (a) and (b) over K. In (a), the colors run from 0 to 4700 m^{-2} and in (b), from 0 to 4200 m^{-2}. The non-intuitive units result in $\mathrm{W/m}^3$ after performing the integrations in Eq. (1).

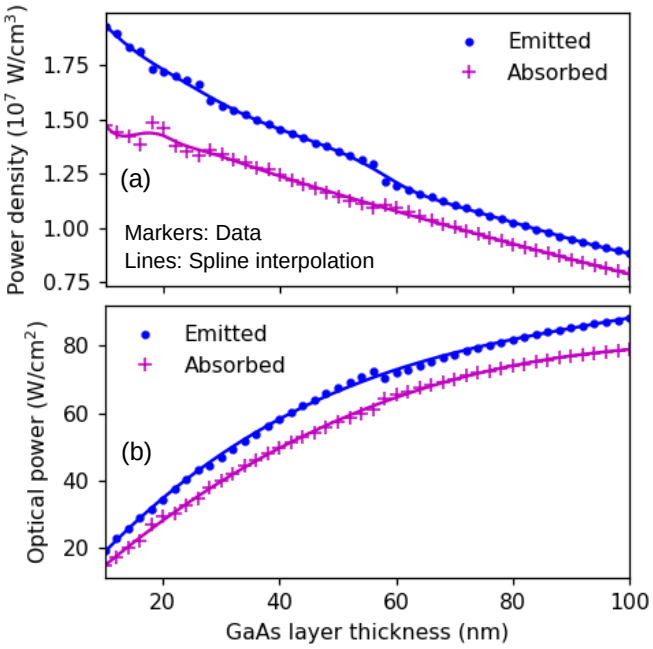

FIG. 5: (a-b) Information in Fig. 2(a-b), respectively, plotted through the vertical arrow in Fig. 2(a). In other words, the figure shows the power density and total optical power in a 265 nm thick cavity as a function of the emitting GaAs layer thickness.

there needs to be more than 650 nm, i.e., the thickness of the GaAs layers and nanogap combined). This indicates that thanks to resonance effects, thinning the active layer to one tenth of such a reference thickness decreases its emission by only 3-4 times. This effect is analyzed more in one of the following paragraphs. Note also that in Fig. 3, the 30 nm thick GaAs absorber layer absorbs almost all the radiation emitted by the emitter, despite being extremely thin. This would naturally not be the case without the intracavity structure having mirrors on both sides, and therefore placing also the detector in a thin-film cavity points to interesting additional material- and cost-saving possibilities. This observation would also motivate a follow-up study focusing on eventual load matching conditions between the emitter and absorber.

For additional insight, next we study the optical mode structure of the cases that exhibit roughly the largest and smallest optical powers in Fig. 3. For this, Fig. 4 shows the spectral recombination rate $r(z, K, \omega)$ averaged over the emitter layer as a function of photon energy and propagation angle (in GaAs) for cavity thicknesses of (a) 265 nm and (b) 370 nm, both with a GaAs layer thickness of 30 nm. It can be seen that thanks to the cavity, light is emitted only into rather discrete angles, with two TE and two TM modes present at both cavity thicknesses. The locations of these modes are not easily explained, but they follow from the numerical solution of Maxwell's equations. However, we note that we have carried out the calculations also without the nanogap (results not shown), and there the TE and TM modes are similarly discrete but they take place at angles corresponding to simple cavity resonance conditions. We expect the position and thickness of the nanogap and the material surrounding it to have notable consequences on the total energy transfer, but studying such dependencies is out of the scope of the present work. Here, referring to the caption, it is seen that Fig. 4(a) shows larger spectral recombination rates than Fig. 4(b). Furthermore, Fig. 4(c) shows the emission spectra of the two cases calculated by integrating Figs. 4(a)-(b) over K. The maximum value of the structure with $d_{Cav} = 265$ nm is roughly 1.5 times the value for $d_{Cav} = 370$ nm, matching well with the difference between these cases observed in Fig. 3. However, it does not seem straightforward to find more qualitative generalizations for the non-monotonous behavior observed in Fig. 3, even if exact relations between the geometry and optical mode structure are behind it.

Finally to answer question (3) and to study how the

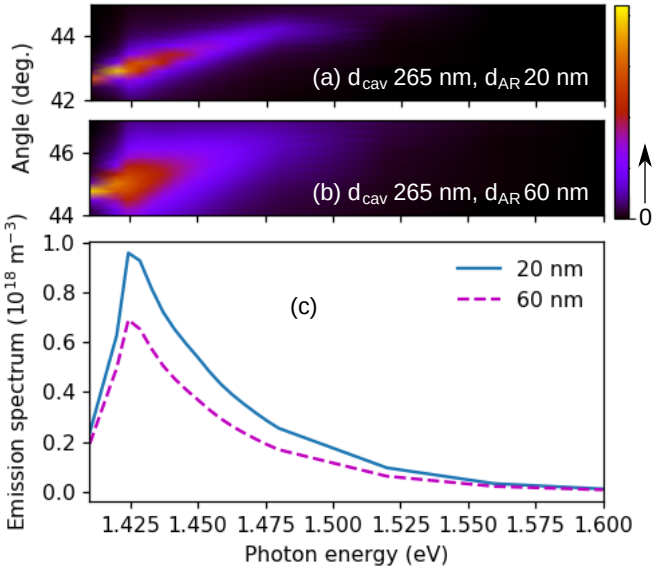

FIG. 6: (a-b) Spectral recombination rate $r(z, K, \omega)$ averaged over the emitter layer and shown for a selected TE mode, with the cavity and GaAs layer thicknesses given in the figures. The emission spectra of the cases considered in (a)-(b) are shown in (c), calculated by integrating $r(z, K, \omega)$ over K. In (a), the colors run from 0 to 5000 m^{-2} and in (b), from 0 to 2000 m^{-2}.

GaAs layer thickness affects the total emission rates, Fig. 5 repeats the information of Fig. 2 along the vertical line shown in Fig. 2(a), i.e., by fixing the cavity thickness and varying the GaAs layer thickness. Figure 5(a) shows in more quantitative terms how R_{rad} decreases with the increasing GaAs layer thickness, essentially due to the increasing reabsorption of the emitted power elsewhere in the emitter layer. As with Fig. 3, the small abrupt changes in the datapoints are expected to result from carrying out the integrations numerically over gradually shifting and broadening emission/absorption peaks. In Fig. 5(b), on the other hand, we see that while the total optical power integrated over the GaAs layer increases with the layer thickness, the increase is sublinear and starts to saturate rather early as a function of the GaAs layer thickness. For example, tripling the GaAs layer thickness from 20 to 60 nm only roughly doubles the optical power. This is explored shortly with help of the optical modes in Fig. 6, which shows $r(z, K, \omega)$ averaged over the emitter layer for a selected TE mode with the GaAs layer thicknesses (a) 20 nm and (b) 60 nm as a function of photon energy and propagation angle. Here, we see that by increasing the GaAs layer thickness from 20 to 60 nm, $r(z, K, \omega)$ both reaches a smaller maximum value (see caption) and exhibits a larger angular spread. The other modes are not shown for brevity, but also they show similar broadening when increasing the GaAs layer thickness from 20 to 60 nm. The spectra in Fig. 6(c) confirm that this effect persists even after integrating over K, which explains the decrease observed in Fig. 5(a) and the sublinear behavior in Fig. 5(b). In other words, a thinner layer emits more strongly and with a smaller angular spread to its discrete modes, and this enhancement effect persists after integrating over K and ω. Furthermore, based on Fig. 5(a), decreasing the GaAs layer thickness might lead to an increasing internal quantum efficiency, if the bulk nonradiative recombination rate densities are assumed to remain constant.

This work provided insight into emission and absorption enhancement of thermal and superluminescent radiation in thin layers and optical cavities, but some important topics were left to future studies. For example, the effect of below-bandgap photons and their role in heat transfer was not considered in detail in this study, as motivated by a simple calculation: Stefan-Boltzmann law suggests that pure thermal emission would only amount to roughly 0.15 $\mathrm{W/cm}^2$ at 400 K, and 1.5 $\mathrm{W/cm}^2$ even when the refractive index of AlGaAs is factored into the calculation (note that this corresponds to ideal emissivity and accounts for all photon energies; near-field heat transfer can increase these numbers due to surface phonon polaritons, but their study and possible optimization is out of the scope of this work). In-plane wave numbers above $1.05 \times N_{GaAs} k_0$ would also need to be considered to properly understand e.g. additional near-field mirror losses and the above-mentioned near-field heat exchange effects across the nanogap. Also, to get quantitative predictions e.g. for device optimization, temperature-adjusted accurate dielectric functions should be used for the semiconductor layers and mirrors, also extending the photon energy grid to smaller values to accurately account for subbandgap absorption. We note that spectral matching between the emitter and absorber layer could then be achieved by properly chosen AlGaAs or InGaAs alloys, and the increased Ag mirror losses could be reduced, e.g., by instead deploying carefully designed distributed Bragg reflectors.

In conclusion, we carried out fluctuational electrodynamics calculations of intracavity structures to study how the radiation transfer between emitter and absorber layers separated by a vacuum nanogap and bordered by high-efficiency mirrors is modified by resonance effects. It was found that even after integrating over wavelength and energy, the total optical power present in the cavity has a strong dependency on both the cavity thickness and the active layer thickness thanks to interference and emission enhancement effects. The results provide a quantitative starting point for further energy transfer studies, where e.g. the proper load matching conditions between the absorber and emitter, the different thermophotonic operation modes, as well as the effect of mirrors are optimized.

Acknowledgments

We acknowledge financial support from the European Union's Horizon 2020 programme (grant agree-

ments 951976 and 964698). The calculations were performed using the computational resources provided by the Aalto Science-IT project.

[1] K. Lehovec, C. A. Accardo, and E. Jamgochian, Light emission produced by current injected into a green silicon-carbide crystal, Phys. Rev. **89**, 20 (1953).
[2] J. Tauc, The share of thermal energy taken from the surroundings in the electro-luminescent energy radiated from a p–n junction, Czech. J. Phys **7**, 275 (1957).
[3] R. J. Keyes and T. M. Quist, Recombination radiation emitted by gallium arsenide, Proc. IRE **50**, 1822 (1962).
[4] G. C. Dousmanis, C. W. Mueller, H. Nelson, and K. G. Petzinger, Evicence of refrigerating action by means of photon emission in semiconductor diodes, Phys. Rev. **133**, A316 (1964).
[5] T. Sadi, I. Radevici, and J. Oksanen, Thermophotonic cooling with light-emitting diodes, Nat. Photon. **14**, 205 (2020).
[6] P. Santhanam, D. J. Gray, Jr., and R. J. Ram, Thermoelectrically Pumped Light-Emitting Diodes Operating above Unity Efficiency, Phys. Rev. Lett. **108**, 097403 (2012).
[7] J. Legendre and P.-O. Chapuis, GaAs-based near-field thermophotonic devices: Approaching the idealized case with one-dimensional PN junctions, Sol. Energ. Mat. Sol. Cells **238**, 111594 (2022).
[8] I. Radevici, J. Tiira, T. Sadi, S. Ranta, A. Tukiainen, M. Guina, and J. Oksanen, Thermophotonic cooling in GaAs based light emitters, Appl. Phys. Lett. **114**, 051101 (2019).
[9] C. Lucchesi, D. Cakiroglu, J.-P. Perez, T. Taliercio, E. Tournié, P.-O. Chapuis, and R. Vaillon, Near-Field Thermophotovoltaic Conversion with High Electrical Power Density and Cell Efficiency above 14%, Nano Lett. **21**, 4524 (2021).
[10] A. Kohiyama, M. Shimizu, K. Konno, T. Furuhashi, and H. Yugami, Effective photon recycling in solar thermophotovoltaics using a confined cuboid emitter, Opt. Express **28**, 38567 (2020).
[11] J. Song, J. Jang, M. Lim, M. Choi, J. Lee, and B. J. Lee, Thermophotovoltaic Energy Conversion in Far-to-Near-Field Transition Regime, ACS Photon. **9**, 1748 (2022).
[12] A. LaPotin, K. L. Schulte, M. A. Steiner, K. Buznitsky, C. C. Kelsall, D. J. Friedman, E. J. Tervo, R. M. France, M. R. Young, A. Rohskopf, S. Verma, E. N. Wang, and A. Henry, Thermophotovoltaic efficiency of 40%, Nature **604**, 287 (2022).
[13] D. Fan, T. Burger, S. McSherry, B. Lee, A. Lenert, and S. R. Forrest, Near-perfect photon utilization in an air-bridge thermophotovoltaic cell, Nature **586**, 237 (2020).
[14] R. Mittapally, B. Lee, L. Zhu, A. Reihani, J. W. Lim, D. Fan, S. R. Forrest, P. Reddy, and E. Meyhofer, Near-field thermophotovoltaics for efficient heat to electricity conversion at high power density. Nat. Commun. **12**, 4364 (2021).
[15] L. Zhu, A. Fiorino, D. Thompson, R. Mittapally, E. Meyhofer, and P. Reddy, Near-field photonic cooling through control of the chemical potential of photons, Nature **566**, 239 (2019).
[16] A. Datas and R. Vaillon, Thermionic-enhanced near-field thermophotovoltaics for medium-grade heat sources, Appl. Phys. Lett. **114**, 133501 (2019).
[17] A. Pusch, J. M. Gordon, A. Mellor, J. J. Krich, and N. J. Ekins-Daukes, Fundamental Efficiency Bounds for the Conversion of a Radiative Heat Engine's Own Emission into Work, Phys. Rev. Appl. **12**, 064018 (2019).
[18] A. Bellucci, P. García-Linares, A. Martí, D. M. Trucchi, and A. Datas, A Three-Terminal Hybrid Thermionic-Photovoltaic Energy Converter, Adv. Energ. Mat. **12**, 2200357 (2022).
[19] M. P. Hehlen, J. Meng, A. R. Albrecht, E. R. Lee, A. Gragossian, S. P. Love, C. E. Hamilton, R. I. Epstein, and M. Sheik-Bahae, First demonstration of an all-solid-state optical cryocooler, Light: Science & Appl. **7**, 15 (2018).
[20] H.-L. Chen, A. Cattoni, R. De Lépinau, A. W. Walker, O. Höhn, D. Lackner, G. Siefer, M. Faustini, N. Vandamme, J. Goffard, B. Behaghel, C. Dupuis, N. Bardou, F. Dimroth, and S. Collin, A 19,9%-efficient ultrathin solar cell based on a 205-nm-thick GaAs absorber and a silver nanostructured back mirror, Nat. Energy **4**, 761 (2019).
[21] M. van Eerden, J. van Gastel, G. J. Bauhuis, P. Mulder, E. Vlieg, and J. J. Schermer, Observation and implications of the Franz-Keldysh effect in ultrathin GaAs solar cells, Prog. Photovolt.: Res. Appl. **28**, 779 (2020).
[22] M. van Eerden, J. van Gastel, G. J. Bauhuis, E. Vlieg, and J. J. Schermer, Comprehensive analysis of photon dynamics in thin-film GaAs solar cells with planar and textured rear mirrors, Sol. Energ. Mat. Sol. Cells **244**, 111708 (2022).
[23] H. Helmers, E. Lopez, O. Höhn, D. Lackner, J. Schön, M. Schauerte, M. Schachtner, F. Dimroth, and A. W. Bett, 68.9% Efficient GaAs-Based Photonic Power Conversion Enabled by Photon Recycling and Optical Resonance, Phys. Stat. Solidi RRL **15**, 2100113 (2021).
[24] S. McSherry, T. Burger, and A. Lenert, Effects of narrowband transport on near-field and far-field thermophotonic conversion, J. Photon. Energy **9**, 032714 (2019).
[25] M. Partanen, T. Häyrynen, J. Tulkki, and J. Oksanen, Commutation-relation-preserving ladder operators for propagating optical fields in nonuniform lossy media, Phys. Rev. A **92**, 033839 (2015).
[26] P. Kivisaari, M. Partanen, T. Sadi, and J. Oksanen, Interplay of Photons and Charge Carriers in Thin-Film Devices, Phys. Rev. Appl. **16**, 024036 (2021).
[27] P. Kivisaari, M. Partanen, and J. Oksanen, Optical admittance method for light-matter interaction in lossy planar resonators, Phys. Rev. E **98**, 063304 (2018).
[28] P. Würfel, The chemical potential of radiation, J. Phys. C. **15**, 3967 (1982).
[29] E. D. Palik, in *Handbook of Optical Constants in Solids,* edited by E. D. Palik (Academic Press, San Diego, 1998), p. 429.
[30] O. J. Glembocki and K. Takarabe, in *Handbook of Optical Constants in Solids,*, edited by E. D. Palik (Academic Press, San Diego, 1998), p. 513.

[31] E. D. Palik, in *Handbook of Optical Constants in Solids*, edited by E. D. Palik (Academic Press, San Diego, 1998), p. 350.